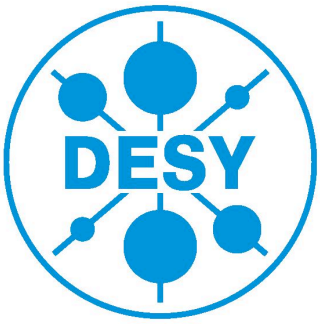

Search for Dark Matter in dileptonic $t\bar{t}$ decays using spin information

Daniela Köck

Supervisors: Dr. Alexander Grohsjean, Dr. Christian Schwanenberger

September 2015

Abstract

To enhance the sensitivity of searches for new physics at the LHC, a set of novel observables that systematically explores all spin information of dileptonic $t\bar{t}$ events has been studied. The performance of the observables has been benchmarked examining $t\bar{t}$ associated dark matter production at $\sqrt{s} = 13$ TeV proton-proton collisions. It is found that on one-hand they allow to better separate the new physics signal from the standard model (SM) background, and on the other-hand, they are highly sensitive to the nature of the new physics. Assuming, for example, that the DM particles couple to the SM fermions through either a scalar or pseudoscalar mediator, the nature of these couplings can be clearly distinguished. In a final step, one of the new observables has been compared to recent data from the CMS experiment at 13 TeV.

Contents

1. Introduction

Altough top quarks are produced almost unpolarised in the standard model (SM) of particle physics, their spins are correlated. As the top quark decays before hadronisation its spin information is fully transmitted to its decay products. Moreover, the decay time of the top is mostly too short for the top spin to be depolarised. Thus, $t\bar{t}$ spin correlation can be measured by analyzing angular distibutions of top decay products. As leptons have the highest spin analyzing power, dileptonic $t\bar{t}$ events, in which both W bosons from the $t \to Wb$ decay decay into a lepton and the corresponding neutrino has been used. Compared to semileptonic final states in which one W boson decays hadronically and one leptonically, dilepton final states have the smallest branching ratio but the lowest fraction of background contamination.
The spins of top (t) and anti-top ($\bar{t}$) are dominately parallel when produced in quark-anti-quark annihilation far from the threshold, e.g. at the Tevatron, whereas they are mainly anti-parallel when produced in gluon-gluon fusion far from threshold, e.g. at the LHC [6]. Processes beyond the SM influence the measured correlation strength, as for example through the emission of a new scalar or pseudoscalar particle, so that spin-based observables are highly sensitive to new physics. In this analysis, of particular interest is the investigation of Dark Matter (DM) models [1, 5]. A sensitivity study of spin and polarisation observables is presented in 13 TeV proton-proton collision samples, taken from Monte Carlo simulations and data collected at the CMS experiment.
The report is structured as follows. First, a short summary of the analysis strategy and selection cuts is given. Then the kinematic event reconstruction is described and the construction of novel spin-based observables as well as their sensitivity are discussed. The report concludes with a comparison to 13 TeV data taken at the CMS experiment.

2. The two lepton analysis

2.1. Data and simulated samples

The summer student project presented here was carried out in the framework of the dileptonic top-antitop ($t\bar{t}$) analysis performed by the CMS group at DESY Hamburg. Of particular interest for this analysis is the

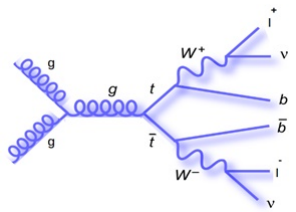

Figure 2.1: Dileptonic Standard Model $t\bar{t}$ decay

process shown in Fig. 2.1, leading to a final state with two opppositely charged leptons, two b-quarks and two undetected neutrinos.

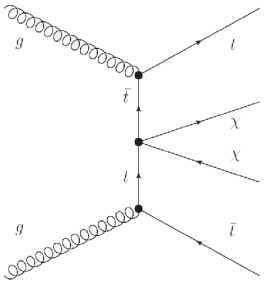

Figure 2.2: Dark Matter associated $t\bar{t}$ -decay [2]

By examining the spin correlation between both leptons, hints of physics beyond the SM (BSM) could be found. In this project, the influence of $t\bar{t}$ associated DM production as shown in Fig. 2.2 is investigated. Not directly shown in this scetch is the mediator particle that connects the DM particles with the SM fermions. To describe the production of DM associated production and the kinematics of the process, so called simplified models are used. In the models investigated here, the couplings to the SM and DM particles are set to 1. The masses of the mediator and the DM particles are treated as free parameters and different Monte-Carlo samples with different mass parameters has been used.

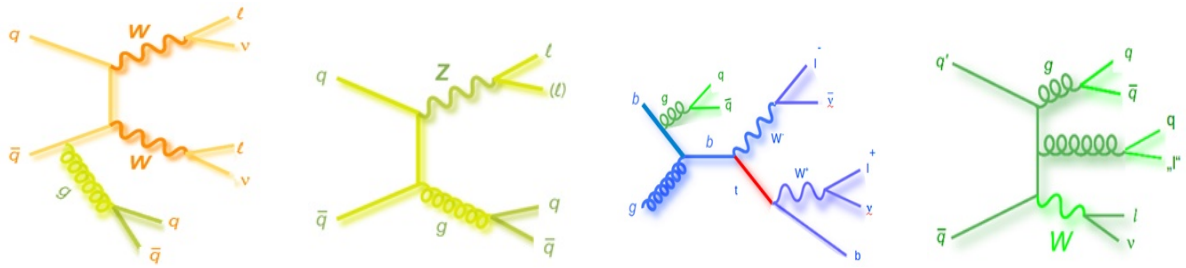

(a) Diboson (b) Drell-Yann (c) Single top (d) W plus Jets

Figure 2.3: Examples of background processes

Searching for $t\bar{t}$ associated DM production, SM $t\bar{t}$ events represent the largest background. Examples of non $t\bar{t}$ processes leading to a similar final state are shown in Fig. 2.3.
This backgrounds could be arranged into four categories:

- non-prompt W: $t\bar{t}$ events others than dilepton, W+jets processes
- Diboson: WW, WZ, ZZ
- Drell Yan processes: Z+jets
- Single top production: t+W and $\bar{t}$+W

The non-prompt W background category contains all events in which a jet is faking a lepton. This could be either an electron that is misidentified as a jet or a muon from a heavy hadron decay inside a jet that appears to be isolated.
The expected SM backgrounds and DM signals are generated with Monte-Carlo simulations. The sample names are summarized in the appendix A.

2.2. Object and event selection

The considered $t\bar{t}$ final state is characterized by the presence of a high-p_T isolated electron-muon pair associated with missing transverse energy and 2 b-quark jets. The reconstruction of the different objects is based on the Particle-Flow (PF) algorithm. The object selection follows the strategy used for the first $t\bar{t}$ cross section measurement at 13 TeV at the CMS experiment [3]. The selected leptons are required to be of opposite charge. Besides being of good quality, p_{T} and η requirements as summarized in Tab. 2.4 are applied to electrons, muons and jets. Later, when comparing data to MC simulations, additional event selection cuts aiming at an efficient supression of background, are introduced. This is further detailed in Sec. 6.

electrons	muons	jets
$p_T \geq 20GeV$	$p_T \geq 20GeV$	$p_T \geq 25GeV$
$\lvert\eta\rvert \leq 2.4$	$\lvert\eta\rvert \leq 2.4$	$\lvert\eta\rvert \leq 2.4$
$\lvert\eta\rvert$ not in $]1.442, 1.5560[$		no overlap with e, μ in $\Delta R = 0.4$

Figure 2.4: Object selections for electrons, muons and jets

3. Kinematic reconstruction

3.1. Reconstruction algorithm

The aim of this project was to test the sensitivity of several novel observables exploring spin and polarization-induced effects in $t\bar{t}$ production as further detailed in Sec. 4. To construct these observables, the full kinematics of the $t\bar{t}$ final state needs to be reconstructed. This is particularly challenging in the dilepton final state because of the two undetected neutrinos escaping the detector. The $t\bar{t}$ event was reconstructed using an algebraic approach. A more detailed explanation can be found in Ref. [4].

The event reconstruction goes back to solving the following set of equations

$$\begin{aligned}
\not{E}_x &= p_{\nu_x} + p_{\bar{\nu}_x} \\
\not{E}_y &= p_{\nu_y} + p_{\bar{\nu}_y} \\
E_\nu^2 &= m_\nu^2 + p_{\nu_x}^2 + p_{\nu_y}^2 + p_{\nu_z}^2 \\
E_{\bar{\nu}}^2 &= m_{\bar{\nu}}^2 + p_{\bar{\nu}_x}^2 + p_{\bar{\nu}_y}^2 + p_{\bar{\nu}_z}^2 \\
m_{W^+}^2 &= (E_{\ell^+} + E_\nu)^2 - (p_{\ell_x^+} + p_{\nu_z})^2 - (p_{\ell_y^+} + p_{\nu_y})^2 - (p_{\ell_z^+} + p_{\nu_z})^2 \\
m_{W^-}^2 &= (E_{\ell^-} + E_{\bar{\nu}})^2 - (p_{\ell_x^-} + p_{\bar{\nu}_z})^2 - (p_{\ell_y^-} + p_{\bar{\nu}_y})^2 - (p_{\ell_x^-} + p_{\bar{\nu}_x})^2 \\
m_t^2 &= (E_b + E_{\ell^+} + E_\nu)^2 - (p_{b_x} + p_{\ell_x^+} + p_{\nu_x})^2 - (p_{b_y} + p_{\ell_y^+} + p_{\nu_y})^2 - (p_{b_z} + p_{\ell_z^+} + p_{\nu_z})^2 \\
m_{\bar{t}}^2 &= (E_{\bar{b}} + E_{\ell^-} + E_{\bar{\nu}})^2 - (p_{\bar{b}_x} + p_{\ell_x^-} + p_{\bar{\nu}_x})^2 - (p_{\bar{b}_y} + p_{\ell_y^-} + p_{\bar{\nu}_y})^2 - (p_{\bar{b}_x} + p_{\ell_x^-} + p_{\bar{\nu}_x})^2
\end{aligned} \tag{3.1}$$

which is achieved by assuming:

- mass-less leptons and neutrinos
- the b-jet mass corresponds to the b-quark mass
- the reconstructed invariant lepton-neutrino mass is 80.4 GeV
- the reconstructed top/anti-top mass is 172.5 GeV

The event reconstruction is done for all possible jet-lepton combinations. Using the exact measured jet and lepton momenta, many events have no solution. This can be overcome by smearing the object momenta within the given detector resolution. Every event is reconstructed 100 times with different smearings, selecting the solution with the minimal invariant $t\bar{t}$ mass.

3.2. Performance check of the kinematic event reconstruction

To assess the performance of the kinematic event reconstruction, resolution plots have been made, see Fig. 3.1. These plots are based on the difference between the 'truth' generator level information and the reconstructed event information. Background suppresion cuts have been applied (see section 6), however the behaviour of the resolution is little affected by this.
As it can be clearly seen in Fig. 3.1, the resolution of both the top transverse momentum and the top pseudorapidity is not ideal and a fairly broad distribution is obtained. To optimize the performance, the event reconstruction needs to be better adjusted to the needs of the high centre-of-mass energy of the LHC. One way to achieve this would be to explicitly include the radiation of the first additional jet into the method.

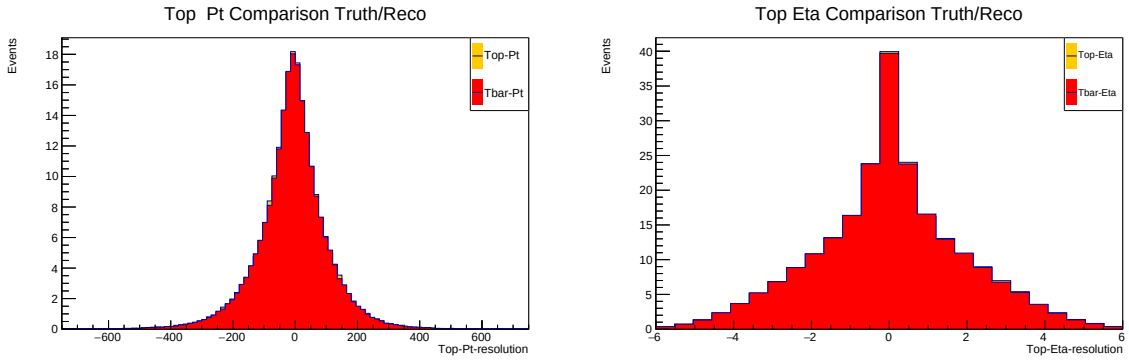

Figure 3.1: Resolution of the reconstructed top transverse momentum (left) and pseudo-rapidity (right).

4. Observables

The most fundamental approach to study all spin and polarization-induced efffects in $t\bar{t}$ production is based on the decomposition of the $t\bar{t}$ spin density matrix. This method and the performance of the associated observables is discussed in the following.

4.1. The $t\bar{t}$ spin density matrix

As shown in detail in Ref. [7], the $t\bar{t}$ spin density matrix can be decomposed into the spin spaces of the top and the anti-top:

$$R^I \propto A^I \mathbb{1} \otimes \mathbb{1} + \tilde{B}_i^{I+} \sigma^i \otimes \mathbb{1} + B_i^{I-} \mathbb{1} \otimes \sigma^i + \tilde{C}_{ij}^I \sigma^i \otimes \sigma^j \tag{4.1}$$

where $I = gg, q\bar{q}$ represents $t\bar{t}$ production via gluon-gluon fusion and quark-antiquark annihilation, respectively. The first summand of Eq. (4.1) is independent of the top quark spin and determines the cross section. The following two summands dependent on the spin of one of the top quarks, provide information about the transverse and longitudinal polarisation of the top quarks. The last addend summarizes all spin-correlation dependent contributions. Equation (4.1) can be further decomposed into an orthonormal basis, which leads to the set of observables presented in the following. For all observables the following notations are used.

$$\begin{aligned}
\hat{\ell}_+ &\mathrel{\widehat{=}} \text{anti-lepton direction in t restframe} \\
\hat{\ell}_- &\mathrel{\widehat{=}} \text{lepton direction in } \bar{t} \text{ restframe} \\
\hat{p} &\mathrel{\widehat{=}} \text{direction of gluon, beam axis direction} \\
\hat{k} &\mathrel{\widehat{=}} \text{top direction in } t\bar{t} \text{ zero mass frame} \\
\hat{n} &= \hat{p} \times \hat{k}
\end{aligned} \tag{4.2}$$

P-even and CP-even spin correlations

Four of the spin correlation associated observables are even under parity (P) and joint charge and parity transformations (CP):

$$\begin{aligned} c_1 &= \hat{\ell}_+ \cdot \hat{\ell}_- \\ c_2 &= (\hat{p} \cdot \hat{\ell}_+)(\hat{p} \cdot \hat{\ell}_-) \\ c_3 &= (\hat{k} \cdot \hat{\ell}_+)(\hat{k} \cdot \hat{\ell}_-) \\ c_4 &= (\hat{p} \cdot \hat{\ell}_+)(\hat{k} \cdot \hat{\ell}_-) + (\hat{k} \cdot \hat{\ell}_+)(\hat{p} \cdot \hat{\ell}_-) \end{aligned} \tag{4.3}$$

These observables have a non-zero contribution in the SM and are therefore asymmetric, as can be seen in Fig. 4.1. For each observable three different sets of input information are used. Shown in green is the calculation of $c_1 - c_4$ based on truth information before any event selection cut is applied, in red after applying selection cuts. The observable distribution after all cuts using the information from the $t\bar{t}$ event reconstruction is shown in blue. All plots show normalized events on the y-axis.
The distributions of the observables based on truth information with and without selection cuts applied are well consistent with each and a distortion due to the applied event selection cuts is not observed. However, $c_2 - c_4$ show large differences when comparing the case of using truth information compared to reconstructed information, while for $c1$ the performance is pretty similar.

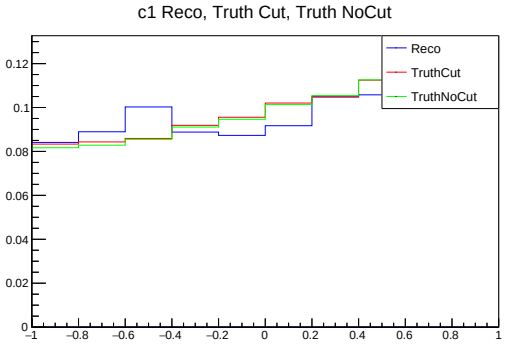

(a) c_1

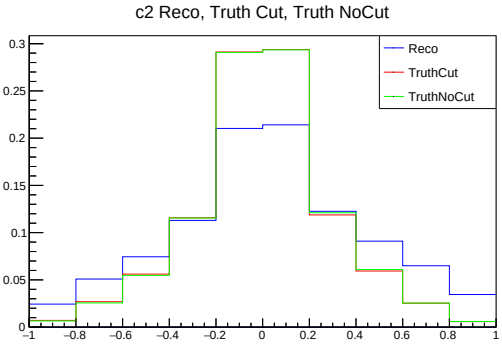

(b) c_2

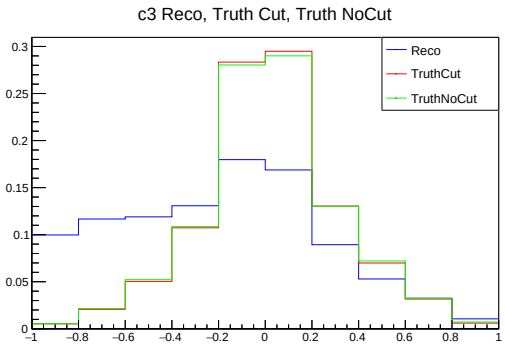

(c) c_3

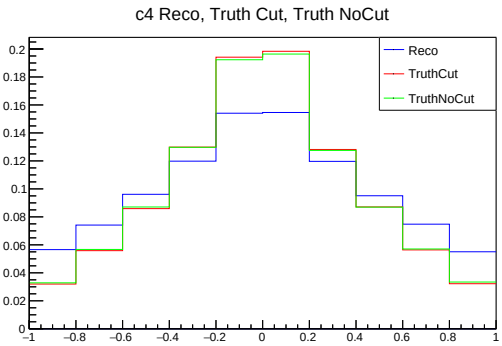

(d) c_4

Figure 4.1: P-even and CP-even spin correlations

P-odd and CP-odd spin correlations

The spin correlations related observables odd under P and CP transformations are c_5 and c_6. These observables are very tiny in the SM as SM $t\bar{t}$ production is P and CP even, which is visible in the symmetric shapes in Fig. 4.2.

$$\begin{aligned} c_5 &= (\hat{\ell}_+ \times \hat{\ell}_-) \cdot \hat{p} \\ c_6 &= (\hat{\ell}_+ \times \hat{\ell}_-) \cdot \hat{k} \end{aligned} \tag{4.4}$$

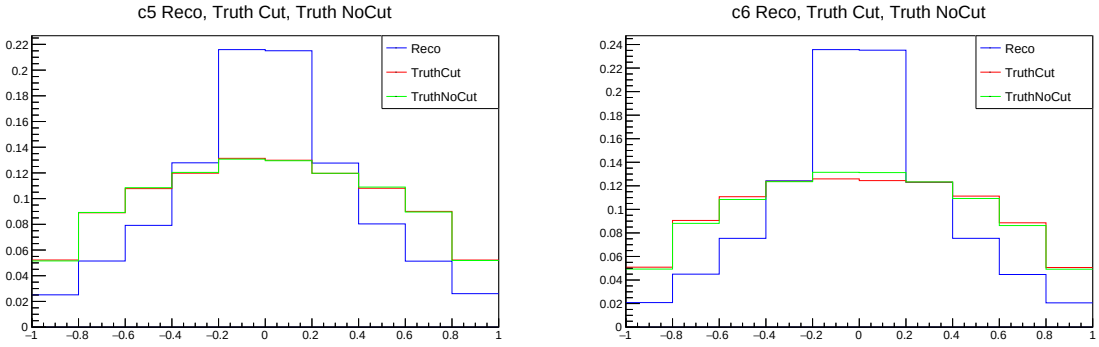

(a) c_5 (b) c_6

Figure 4.2: P-odd and CP-odd spin correlations

P-odd longitudinal polarisation

Top quarks from $t\bar{t}$ production are unpolarized in the longitudinal plane [6]. So the longitudinal polarizations are zero in the SM, as can be seen in Fig. 4.3.

$$b_1 = \hat{p} \cdot \hat{\ell}_+ + \hat{p} \cdot \hat{\ell}_- \tag{4.5}$$

$$b_2 = \hat{k} \cdot \hat{\ell}_+ + \hat{k} \cdot \hat{\ell}_- \tag{4.6}$$

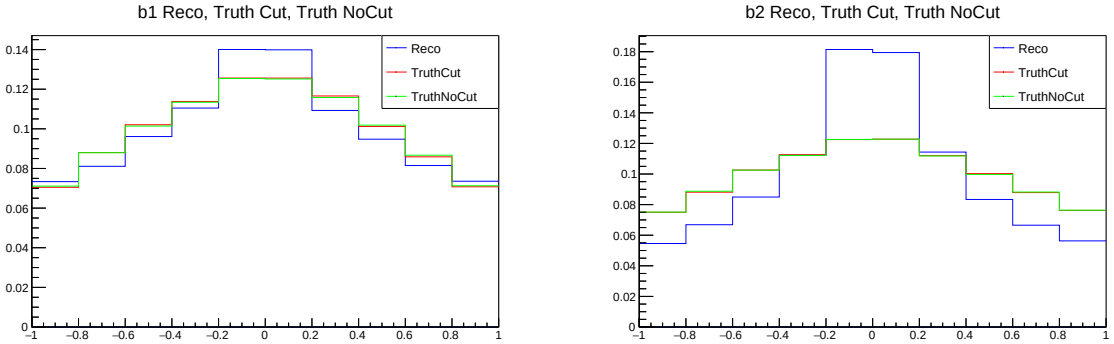

(a) b_1 (b) b_2

Figure 4.3: P-odd longitudinal polarisations

Transverse top- and anti-top polarisation

The transverse polarisation is predicted to be very small, so the shapes in Fig. 4.4 are almost symmetric.

$$\begin{aligned} b_3^+ &= \hat{n} \cdot \hat{\ell}_+ + \hat{n} \cdot \hat{\ell}_- \\ b_3^- &= \hat{n} \cdot \hat{\ell}_+ - \hat{n} \cdot \hat{\ell}_- \end{aligned} \tag{4.7}$$

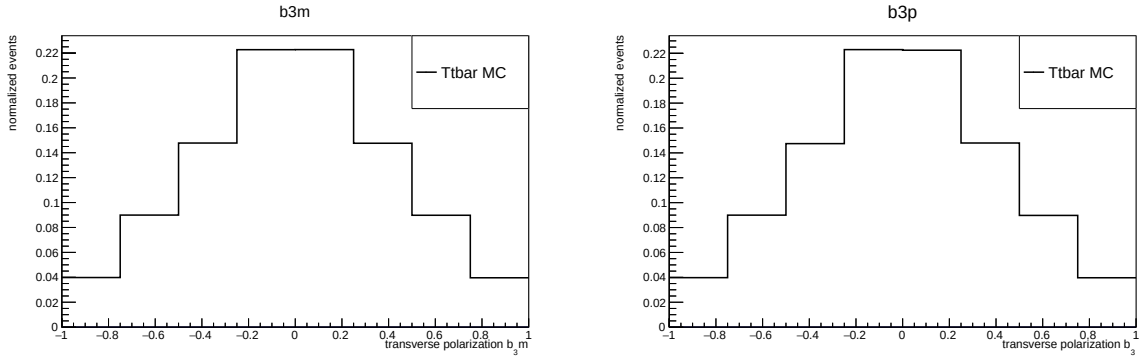

(a) b_3^- (b) b_3^+

Figure 4.4: Transverse top- and anti-top polarisation

4.2. Alternative angle dependent observables

Azimuthal difference - $\Delta\Phi$

The azimuthal angle $\Delta\Phi$ between the two leptons in the laboratory frame, compare Fig. 4.5, is proportional to a linear combination of c_1 and c_4, has highest sensitive to $t\bar{t}$ spin correlations at the LHC, and is very little effected by reconstruction effects.

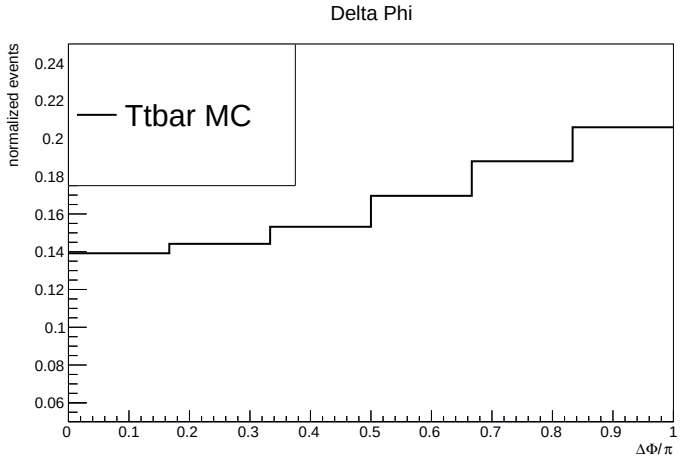

Figure 4.5: Azimuthal difference

Pseudorapidity difference - $\Delta\eta$

Similar to $\Delta\Phi$, the difference in pseudorapidity $\Delta\eta$, compare Fig. 4.6 is measured in the laboratory frame and allows a sensitive probe of new physics in $t\bar{t}$ production without using complex reconstruction algorithms.

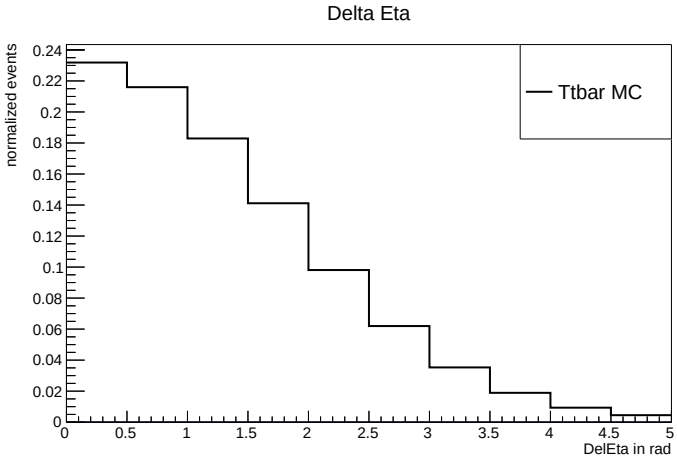

Figure 4.6: Pseudorapidity difference

5. Sensitivity studies

The performance of the above introduced observables in searches for new physics is estimated in the following by comparing the shape of a few observables in $t\bar{t}$ associated DM production and SM $t\bar{t}$ production.

5.1. Reconstruction check

As can already be seen from Fig. 3.1, the kinematic event reconstruction has clear deficits in the reconstruction of the top and anti-top quark. To check the impact on the angular based observables an additional comparison is done in Fig. 5.1, where the angles between the leptons, ℓ^+/ℓ^-, and the corresponding top quarks, $t/\bar{t}$, in the laboratory frame are plotted for SM $t\bar{t}$ production. Again, the shape of the observables differ significantly for the case of using reconstructed event information and truth level information. That means the reconstruction algorithm allows no proper estimate of the top direction and needs a significant revision before the full separation power of the $t\bar{t}$ spin density matrix can be obtained. As already mentioned above a possible reason could be the miss-consideration of the system boost. The reconstruction algorithm is configured for 8 TeV, so the much higher center-of-mass energy of 13 TeV could lead to the wrong reconstruction. This feature has to be further investigated.

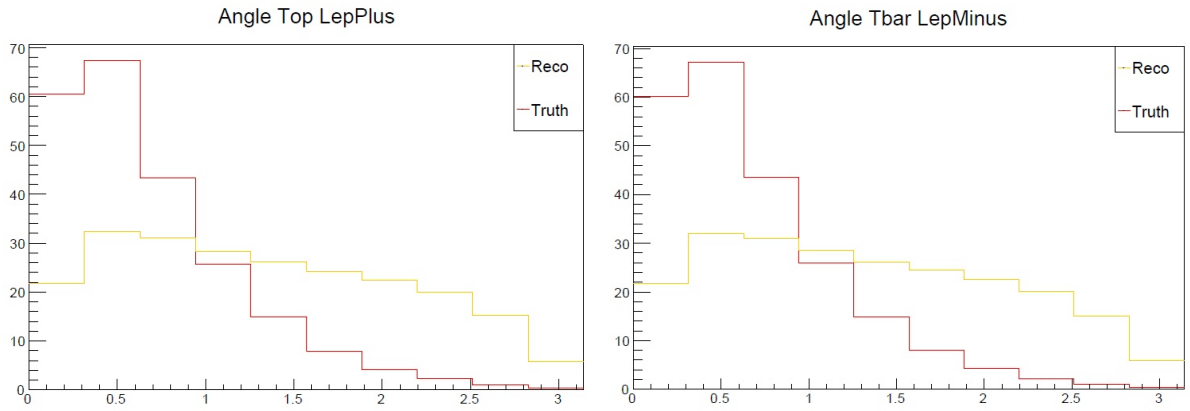

(a) top and anti-lepton

(b) anti-top and lepton

Figure 5.1: Angle in lab system between top (anti-top) and anti-lepton (lepton)

5.2. Truth comparisons

To assess the separation power of the observables in the search for $t\bar{t}$ associated DM production, the shape of the observables is compared between various models of $t\bar{t}$ associated DM production and the dominant background of SM $t\bar{t}$ production. To avoid a possible dilution of performance from the event reconstruction method, all variables are calculated using Monte-Carlo truth information. In the following, three variables are shown exemplarily for all spin and polarization-induced effects. These are the azimuthal angle between two leptons, $\Delta\Phi$, as well as $cos(\theta_{l^+})cos(\theta_{l^-})$ and b_3^+.
A particular interesting aspect of studying spin- and polarization induced effects in searches for new physics is that the observables associated to the $t\bar{t}$ spin density matrix allow a characterization of the new physics in terms of symmetry properties such as P-, CP-, and T-conjugation as well as a first glimpse on the nature of the coupling to the SM. In the juxtaposition shown in Fig. 5.2 (c), an obvious asymmetry can be seen for both cases the scalar and pseudoscalar mediated coupling of the DM particles to the SM, while SM $t\bar{t}$ production is symmetric. The pseudoscalar case shows an asymmetric shape to negative values, whereas the scalar one tends to positive values. Similar, clear differences between the SM case and the two DM models can be observed for spin correlation based observables, as shown in Fig. 5.2 (a) and (b).
In addition to the clear differences between scalar and pseudoscalar couplings, effects from different mediator masses are visible in the angular-based observables, as shown in Fig. 5.3. These effects need to be further studied in future and a combination with additional energy- and kinematic-based observables will be needed to fully pin down the different properties of the new physics. In App. B the same comparison is shown for pseudoscalar models.

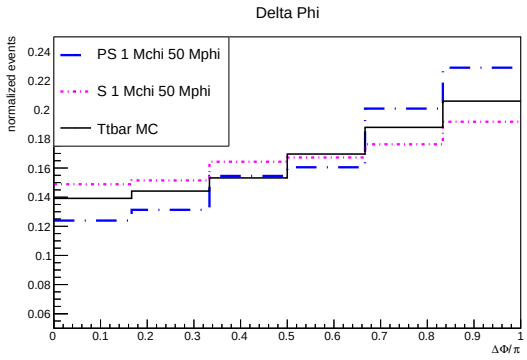

(a) $\Delta\Phi$

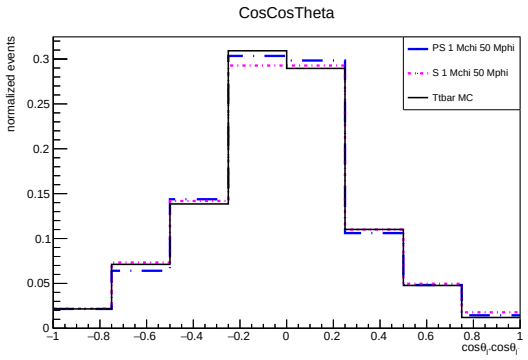

(b) $cos(\theta_{l^+})cos(\theta_{l^-})$

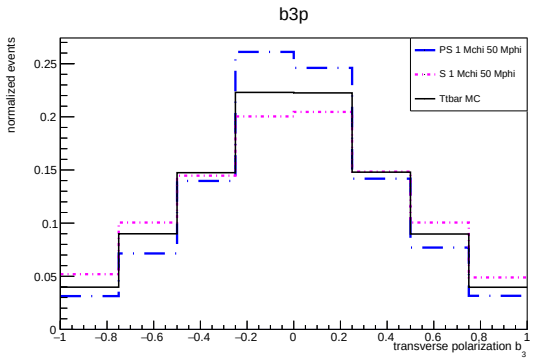

(c) b_3^+

Figure 5.2: Comparison of scalar and pseudoscalar models

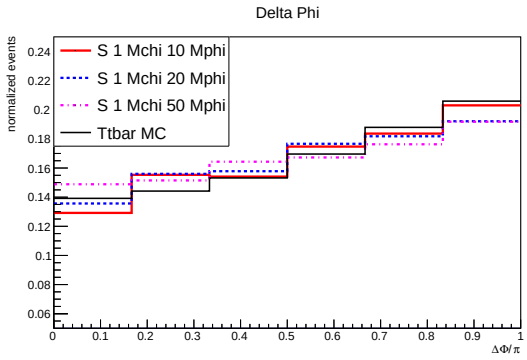

(a) $\Delta\Phi$

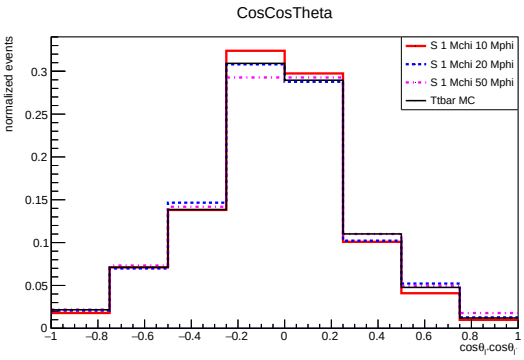

(b) $cos(\theta_{l^+})cos(\theta_{l^-})$

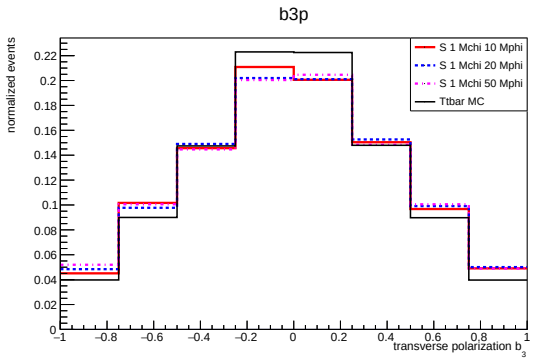

(c) b_3^+

Figure 5.3: Comparison of scalar models with different mediator masses

6. Comparison to data

In addition to the sensitivity studies at the truth level, the azimuthal angle between two leptons has been studied at the reconstruction level in 13 TeV LHC data. Therefore, the full CMS data set recorded in July 2015 with an integrated luminosity of 41.6pb^{-1} has been used. To suppress background contributions from non $t\bar{t}$ background several selection cuts are applied. Firstly, two leptons, one electron and one muon, of opposite charge are required, where the two leptons have to be the highest - p_T leptons. Secondly, the invariant mass of the two leptons, $m_{\ell^+\ell^-}$, has to be greater than 20 GeV. This requirement is used to suppress low-mass Drell-Yan (DY) background where a photon or virtual Z boson decays into a lepton pair. Finally, at least two jets are required which helps to greatly reduce diboson and DY background. The reduction of background events after each cut are shown in Fig. 6.1, where the cuts discussed in Sec. 2.2 are always applied.

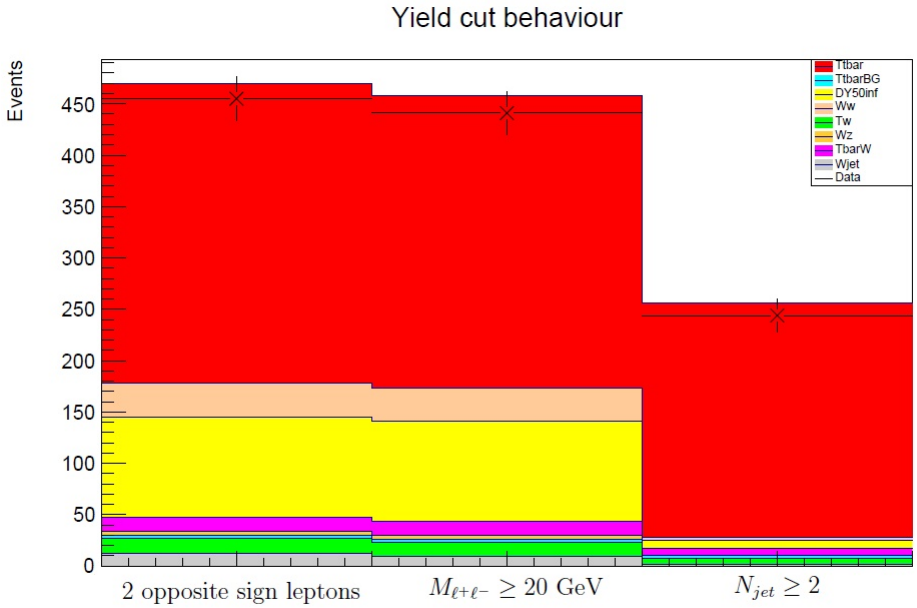

Figure 6.1: Cutflow

In Fig. 6.2 the $\Delta\Phi/\pi$ distribution is shown with all cuts applied. The $t\bar{t}$ +DM sample represented with the dotted bright blue line is normalized to the $t\bar{t}$ cross section to compare the shapes. The backgrounds are sorted in the categories mentioned in Sec. 2.1. Clearly visible is the difference in slope between the dominant $t\bar{t}$ background and the $t\bar{t}$ +DM process demonstrating the high sensitivity and excellent performance of the $\Delta\Phi/\pi$ observable at the reconstruction level. The ratio of data to Monte-Carlo, excluding the $t\bar{t}$ +DM physics signal, is depicted in the lower graph in 6.2. No significant deviation of the collected data from the SM prediction could be observed. For a detailed study

more statistics is needed and uncertainties arrising from the MC simulated samples as well as systematic uncertainties have to be taken into account.

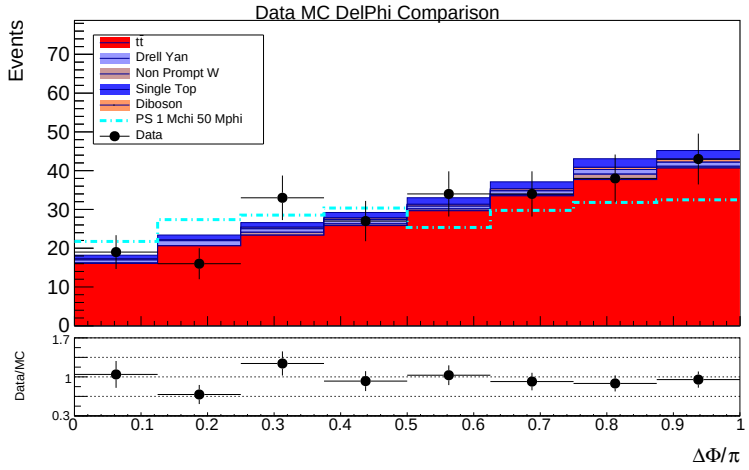

Figure 6.2: Data - MC comparison

7. Conclusion and outlook

A sensitivity study of spin and polarization-based observables in dileptonic ($e^{\pm}\mu^{\mp}$) $t\bar{t}$ events is presented in $\sqrt{s} = 13$ TeV proton-proton collisions. The novel observables result from a decomposition of the $t\bar{t}$ spin density matrix and show excellent separation power between SM $t\bar{t}$ production and $t\bar{t}$ associated DM production. Besides an increased sensitivity to the new physics, they offer access to its nature. As an example, the case of scalar and pseudoscalar couplings of DM particles to SM fermions can be clearly distinguished. An additional study with a full reconstruction of the $t\bar{t}$ event kinematics was presented. To benefit from all observables associated with the $t\bar{t}$ spin density matrix, this reconstruction needs to be further improved and adjusted to the larger boosts at 13 TeV. Finally, a first data to MC comparison of the azimuthal angle between the two leptons was presented. Good agreement between the SM process and the data was observed. Significantly more data are needed to see hints of DM at the LHC or to exclude models of $t\bar{t}$ associated DM production.

Acknowledgments

I would like to thank my supervisors Dr. Alexander Grohsjean and Dr. Christian Schwanenberger for this interesting summer student project. Thanks for taking good care and teaching me such a large amount of top physics and coding during my stay. Also I would like to thank the whole CMS group for being so welcoming and helpful. A great thanks to my office colleague Malin Litwinski for the wonderful team work during this programme.

A. Used Monte Carlo samples

Data

/nfs/dust/cms/user/tarndt/NTuples/Prod_ 746/tree_ 13TeV_ emu.root

Standard Model samples

/nfs/dust/cms/user/tarndt/NTuples/Prod_ 746/tree_ 13TeV_ emuttbar.root
/nfs/dust/cms/user/tarndt/NTuples/Prod_ 746/tree_ 13TeV_ emuttbarbg.root
/nfs/dust/cms/user/tarndt/NTuples/Prod_ 746/tree_ 13TeV_ dy50inf.root
/nfs/dust/cms/user/tarndt/NTuples/Prod_ 746/tree_ 13TeV_ ww.root
/nfs/dust/cms/user/tarndt/NTuples/Prod_ 746/tree_ 13TeV_ tW.root
/nfs/dust/cms/user/tarndt/NTuples/Prod_ 746/tree_ 13TeV_ wz.root
/nfs/dust/cms/user/tarndt/NTuples/Prod_ 746/tree_ 13TeV_ tbarW.root
/nfs/dust/cms/user/tarndt/NTuples/Prod_ 746/tree_ 13TeV_ wjets.root

Dark Matter samples

TTbarDMJets_ pseudoscalar_ Mchi-1_ Mphi-10_ TuneCUETP8M1_ 13TeV-madgraphMLM-pythia8/RunIISpring15DR74-Asympt25ns_ MCRUN2_ 74_ V9-v1/MINIAODSIM
TTbarDMJets_ pseudoscalar_ Mchi-1_ Mphi-20_ TuneCUETP8M1_ 13TeV-madgraphMLM-pythia8/RunIISpring15DR74-Asympt25ns_ MCRUN2_ 74_ V9-v1/MINIAODSIM
TTbarDMJets_ pseudoscalar_ Mchi-1_ Mphi-50_ TuneCUETP8M1_ 13TeV-madgraphMLM-pythia8/RunIISpring15DR74-Asympt25ns_ MCRUN2_ 74_ V9-v1/MINIAODSIM
TTbarDMJets_ pseudoscalar_ Mchi-150_ Mphi-200_ TuneCUETP8M1_ 13TeV-madgraphMLM-pythia8/RunIISpring15DR74-Asympt25ns_ MCRUN2_ 74_ V9-v1/MINIAODSIM
TTbarDMJets_ pseudoscalar_ Mchi-150_ Mphi-500_ TuneCUETP8M1_ 13TeV-madgraphMLM-pythia8/RunIISpring15DR74-Asympt25ns_ MCRUN2_ 74_ V9-v1/MINIAODSIM

TTbarDMJets_pseudoscalar_Mchi-150_Mphi-1000_TuneCUETP8M1_13TeV-madgraphMLM-pythia8/RunIISpring15DR74-Asympt25ns_MCRUN2_74_V9-v1/MINIAODSIM
TTbarDMJets_scalar_Mchi-1_Mphi-10_TuneCUETP8M1_13TeV-madgraphMLM-pythia8/RunIISpring15DR74-Asympt25ns_MCRUN2_74_V9-v1/MINIAODSIM
TTbarDMJets_scalar_Mchi-1_Mphi-20_TuneCUETP8M1_13TeV-madgraphMLM-pythia8/RunIISpring15DR74-Asympt25ns_MCRUN2_74_V9-v1/MINIAODSIM
TTbarDMJets_scalar_Mchi-1_Mphi-50_TuneCUETP8M1_13TeV-madgraphMLM-pythia8/RunIISpring15DR74-Asympt25ns_MCRUN2_74_V9-v1/MINIAODSIM

B. Sensitivity studies - additional comparisons

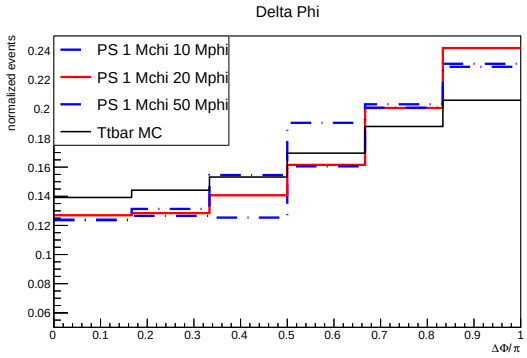

(a) $\Delta\Phi$

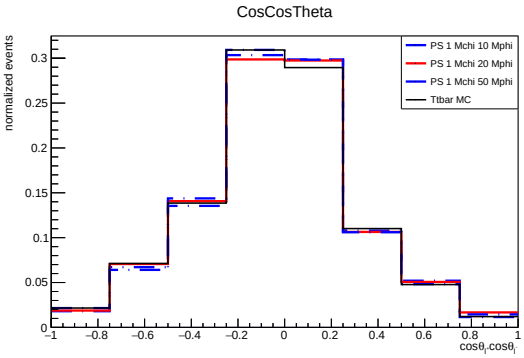

(b) $cos(\theta_{l^+})cos(\theta_{l^-})$

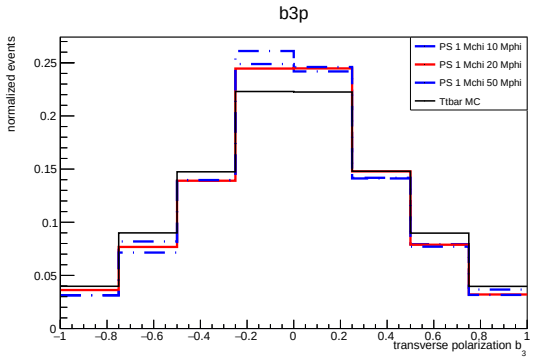

(c) b_3^+

Figure B.1: Comparison of pseudoscalar models with different mediator masses

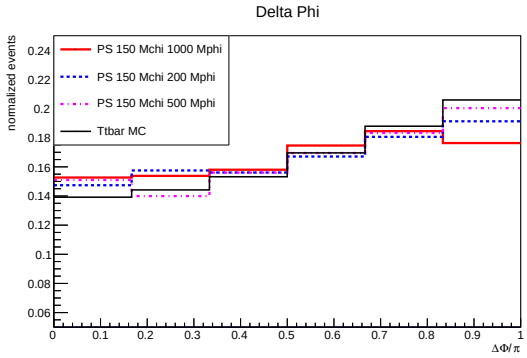

(a) $\Delta\Phi$

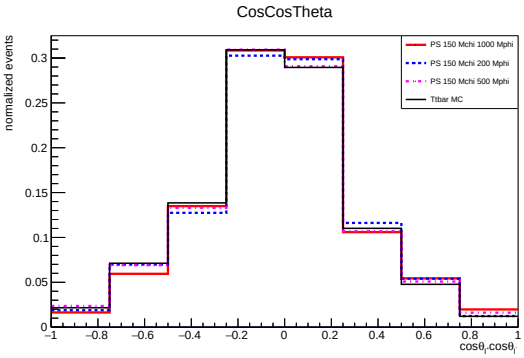

(b) $cos(\theta_{l+})cos(\theta_{l-})$

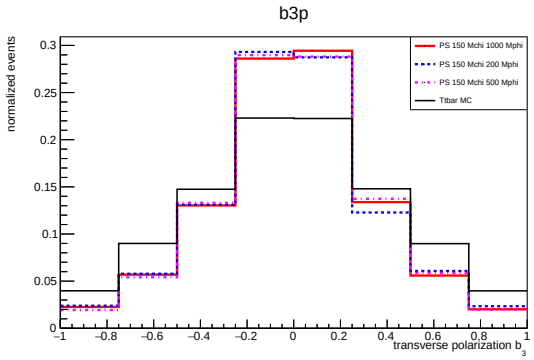

(c) b_3^+

Figure B.2: Comparison of pseudoscalar models with different mediator masses

References

[1] Dark Matter: A Primer *K. Garrett, G. Dũda* (2011)
arXiv:1006.2483v2 [hep-ph]

[2] Search for the Production of Dark Matter in Association with Top Quark Pairs in the Di-lepton Final State in pp collisions at $\sqrt{s} = 8$ TeV
CMS Collaboration (2014)
CMS-PAS-B2G-13-004

[3] Measurement of the top quark pair production cross section in proton-proton collisions at $\sqrt(s) = 13$ TeV
CMS Collaboration (2015)
CMS-TOP-15-003

[4] Analytical solution of $t\bar{t}$ dilepton equations *Lars Sonnenschein* (2011)
arXiv:hep-ph/0603011v3

[5] Simplified dark matter top-quark interactions at the LHC
U. Haisch, E. Re (2015)
arXiv:1503.00691v4 [hep-ph]

[6] Top quark physics at Hadron Colliders *A. Quadt*
Eur. Phys. J. C **48**, 835-1000 (2006)

[7] A set of top quark spin correlation and polarisation observables for the LHC: Standard Model predictions and new physics contributions
W. Bernreuther, D.Heisler, Z. G. Si (2015)
arXiv:1508.05271v1 [hep-ph]

[8] Investigation of Top quark Spin correlations at hadron colliders
W. Bernreuther, A. Brandenburg, Z. G. Si, P. Uwer (2004)
arXiv:hep-ph/0410197

[9] Top quark spin correlations and polarisation at the LHC: standard model predictions and effects of anomalous top chromo moments
W. Bernreuther, Z. G. Si (2015)
arXiv:1305.2066v2